Zhang *et al.*
Journal of NeuroEngineering and Rehabilitation (2024) 21:87
https://doi.org/10.1186/s12984-024-01386-x

Journal of NeuroEngineering and Rehabilitation

RESEARCH

Open Access

Assistance force-line of exosuit affects ankle multidimensional motion: a theoretical and experimental study

Xinyue Zhang[1], Ying Li[1] and Ronglei Sun[1*]

Abstract

Background The talocrural joint and the subtalar joint are the two major joints of the ankle-joint complex. The position and direction of the exosuit force line relative to these two joint axes can influence ankle motion. We aimed to understand the effects of different force-lines on ankle multidimensional motion.

Methods In this article, three assistance force line schemes for ankle exosuits were proposed: perpendicular to the talocrural joint axis (PT), intersecting with the subtalar joint axis (IS), and parallel to the triceps surae (PTS). A theoretical model was proposed to calculate the exosuit's assistance moment. Seven participants completed four experimental tests of ankle plantarflexion, including three passive motions assisted by the PT, PTS and IS schemes, and one active motion without exosuit assistance (Active).

Results The simulation results demonstrated that all three exosuits were able to produce significant moments of ankle plantarflexion. Among these, the PT scheme exhibited the highest moments in all dimensions, followed by the PTS and IS schemes. The experimental findings confirmed the effectiveness of all three exosuit schemes in assisting ankle plantarflexion. Additionally, as the assistive force lines approached the subtalar joint, there was a decrease in ankle motion assisted by the exosuits in non-plantarflexion directions, along with a reduction in the average distance of ankle angle curves relative to active ankle motion. Furthermore, the linear correlation coefficients between inversion and plantarflexion, adduction and plantarflexion, and adduction and inversion gradually converged toward active ankle plantarflexion motion.

Conclusions Our research indicates that the position of the exosuit force line to the subtalar joint has a significant impact on ankle inversion and adduction. Among all three schemes, the IS, which has the closest distance to the subtalar joint axes, has the greatest kinematic similarity to active ankle plantarflexion and might be a better choice for ankle assistance and rehabilitation.

Keywords Ankle exosuit, Assistance force line, Plantarflexion, Inversion, Subtalar joint, Talocrural joint

Background

The ankle plays an important role in generating power and propelling the body forward during movement [1–3]. Ankle exosuits are wearable devices that are designed to enhance human movement performance or aid in ankle rehabilitation [4–7], primarily by assisting ankle plantarflexion motion [8, 9]. To evaluate the effects of these exosuits on ankle function and human gait, a variety of metrics have been proposed. Gait parameters and ankle

*Correspondence:
Ronglei Sun
ronglei@hust.edu.cn
[1] Institute of Medical Equipment Science and Engineering, State Key Laboratory of Intelligent Manufacturing Equipment and Technology, School of Mechanical Science and Engineering, Huazhong University of Science and Technology, Wuhan, China

joint angles are commonly used to assess the impact of exosuits on the ankle and human kinematics [10, 11]. Additionally, ankle joint moment, power, and metabolic power are utilized to evaluate their effects on ankle energy consumption and gait metabolic cost [12–15]. Furthermore, current ankle exosuits research primarily focuses on the sagittal plane motion of the ankle joint, with little attention given to the effects on inversion-eversion and abduction-adduction motion during assisting plantarflexion.

Considering the musculoskeletal anatomy of the ankle-joint complex and the structure of ankle exosuits, ankle non-plantarflexion motion (i.e., ankle eversion/inversion and adduction/abduction) cannot be ignored. As shown in Fig. 1, ankle motion is described in three orthogonal planes: plantar/dorsiflexion along the sagittal plane, inversion/eversion along the frontal plane, and adduction/abduction along the horizontal plane [1, 16, 17]. However, the major rotation joints of the ankle-joint complex are the talocrural and subtalar joints, and their two joint axes are not parallel to the three standard three orthogonal planes [18–20]. Consequently, ankle plantarflexion is not a purely unidirectional motion but is accompanied by a three-dimensional coupling movement [16, 19]. Furthermore, the contraction structures of current exosuits, such as pneumatic muscles or Bowden lines [21], pass through the subtalar joints. Since the subtalar joint is responsible for ankle version/inversion and adduction/abduction [16, 20, 22], ankle exosuits inevitably affect the non-plantarflexion motion of the ankle.

During walking, changes in ankle inversion/eversion moment are applied to counteract deviations in side-to-side center-of-mass acceleration, ensuring balance [23, 24]. An unexpected ankle moment introduced by an exosuit may disrupt the natural ankle movements, resulting in elevated joint loads and biomechanical alterations [25–27]. These disruptions may increase susceptibility to ankle sprains [28–30]. This can be particularly problematic for those who depend on the exosuit to compensate for impaired balance or mobility [31], as it can increase the fear of falling and the incidence of falls [32–34]. Therefore, it is essential to consider the impact of the exosuit on the ankle's natural motion and develop an approach that aligns with multidimensional movement patterns to promote safety.

The effect of an ankle exosuit on multidimensional ankle motion depends on the relationship between the force line and the two ankle axes. In this study, we primarily used the force line to describe the position and direction of the assistive force applied to the talocrural and subtalar joint axes. Several studies have recognized the importance of the position of assistance line force and have employed double or multiple drive cables to assist multidimensional ankle motion (Table 1). These drive cables are positioned in the anterior-posterior position of the ankle joint for ankle plantar/dorsiflexion and the medial-lateral position for inversion/eversion [37, 39, 40], particularly in patients with cerebral palsy and stroke [41]. However, the current study has not sufficiently investigated the effect of the force line on multidimensional ankle motion in the one-cable-drive exosuit designed to assist ankle plantarflexion.

Our study aimed to evaluate the effects of the exosuit force line on ankle kinematics. To achieve this, we developed three force line schemes for ankle exosuits, based on the musculoskeletal anatomy and muscle distribution of the ankle (Fig. 1). The first scheme, PT, was designed to be perpendicular to the talocrural joint axis, while the

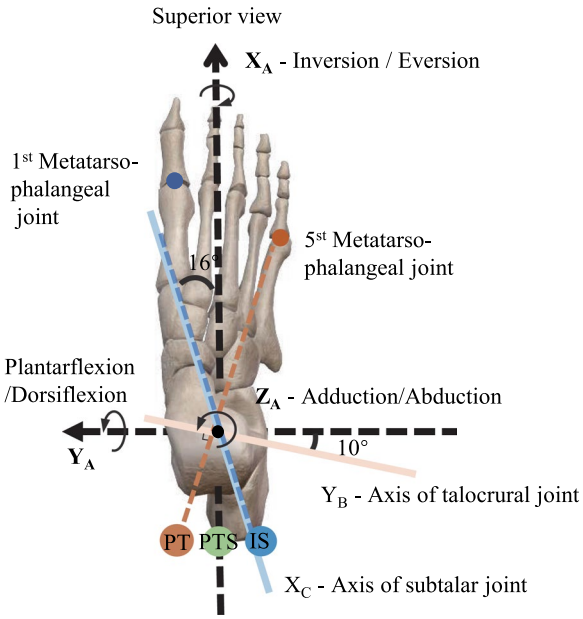

Fig. 1 The ankle joint axes and three assistance force line schemes. The ankle rotation was described using the coordinate system {*A*}. Rotation around the X_A-axis was defined as inversion/eversion, rotation around the Y_A-axis was defined as plantarflexion/dorsiflexion, and rotation around the Z_A-axis was defined as adduction/abduction. The subtalar joint's axis, represented by a solid blue line, is inclined at 16 degrees from the X_A-axis, while the talocrural joint's axis, depicted by a solid orange line, is tilted at 10 degrees from the Y_A-axis. The drive-cable arrangements for the three force line schemes are indicated by the dashed lines. In the PT scheme, the drive cable runs parallel to the calf, then passes the medial side of the heel (orange dot), turns towards the fifth metatarsophalangeal joint along the orange dashed line in the sole, and ultimately fixed to the dorsal surface of the foot. In the PTS scheme, the drive cable runs parallel to the calf and is fixed in the center of the heel (green dot). In the IS scheme, the drive cable is parallel to the calf and directed towards the lateral side of the heel (blue dot), then turns towards the first metatarsophalangeal joint along the blue dashed line in the sole, and ultimately fixed to the dorsal surface of the foot

Table 1 Typical configuration of the drive cable on the foot in cable-drive ankle exosuits

No.	References	DOF[a]	Drive-cable Pos[b]	Functionality	Target Population
1	[4]	1	x^-	Assist plantarflexion	Normal
2	[8]	1	x^-	Assist plantarflexion	Normal
3	[35]	1	x^+	Resist plantarflexion	Rehabilitation
4	[36]	2	x^-,y^-	Assist plantarflexion and eversion	Rehabilitation
5	[37]	2	x^-,x^+	Assist plantar/dorsiflexion	Rehabilitation
6	[38]	2	x^-,x^+	Assist plantar/dorsiflexion	Stroke patients
7	[39]	4	x^-,x^+,y^-,y^+	Assist plantar/dorsiflexion and inversion/eversion	Stroke patients

[a] DOF, which stands for degrees of freedom, is directly related to the number of cable drives in the exosuits

[b] Pos: The position of the ankle exosuit's drive cable on the foot. With the ankle joint rotation center as the reference point, x^+,x^-,y^+,y^- were used to represent the four positions in which the ends of the driving cable are anchored: front, back, left, and right relative to the ankle joint, respectively

second scheme, IS, was designed to intersect with the subtalar joint axis. The third scheme, PTS, was designed to be parallel to the triceps surae, a common design used in most existing exosuits. We hypothesized that the IS scheme had the least impact on the subtalar joint and the greatest kinematic similarity to active ankle plantarflexion compared to the other two schemes. To test this hypothesis, we developed a theoretical model to calculate the exosuit's assistance moment. By comparing ankle assistance moments with and without considering the ankle joint axes, we highlighted the importance of incorporating the physiological ankle axis in exosuit analysis. To evaluate the effects of the exosuit force line on the ankle, we conducted four experimental tests, including three ankle passive motions assisted by the PT, PTS, and IS schemes, and one ankle active motion without exosuit assistance. We compared the peak angle values in three orthogonal directions, the linear correlation coefficients between the inversion angle and plantarflexion angle, between the adduction angle and plantarflexion angle, and between the adduction angle and inversion angle, and the distance of ankle motion between exosuit-assisted and active ankle motion to evaluate the extent to which each exosuit scheme resembled ankle active plantarflexion.

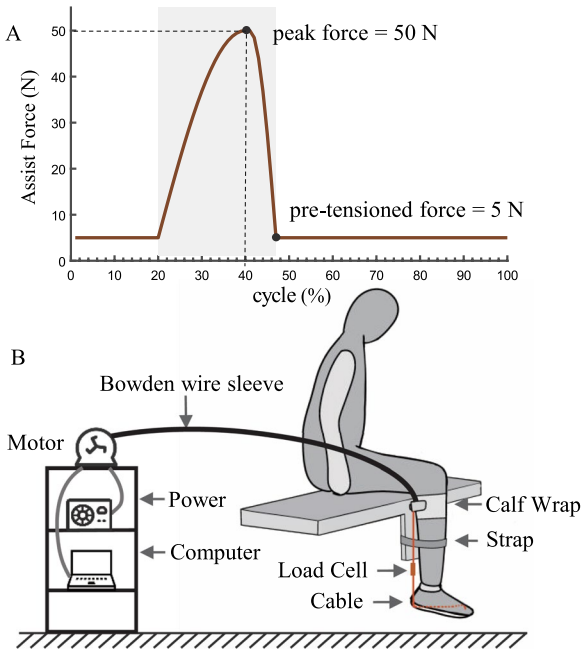

Fig. 2 The ankle exosuit experimental platform. **A** The assist force curve. **B** The ankle exosuit system and experimental protocol. The participant was seated on a platform with the ankle exosuit on the right leg. Assisting force was transmitted to the ankle via Bowden cables, actuated by a motor positioned on the side shelf. The calf was fastened to the platform with straps to prevent knee joint rotation during the experiment

Methods

Ankle exosuit structure design

We developed three force line schemes for ankle exosuits, based on the musculoskeletal anatomy and muscle distribution of the ankle. The Bowden cables originate from the motor reel and are routed through the Bowden cable housing before arriving at the calf wrap located on the posterior aspect of the lower leg. From there, the cables run parallel to the calf and extend to the heel (Fig. 2B), while the assist force was measured using a load cell series connection with the cable. However, the positioning of the cables on the heel and foot sole differs among the three schemes (Fig. 3).

The IS scheme is routed to pass the lateral side of the heel, at a distance of approximately 3 cm from the midpoint of the heel. To ensure durability, a Teflon hose is embedded within the sole of the shoe to house the cable. The cable then passes through this hose to reach the underside of the first metatarsophalangeal joint. Finally,

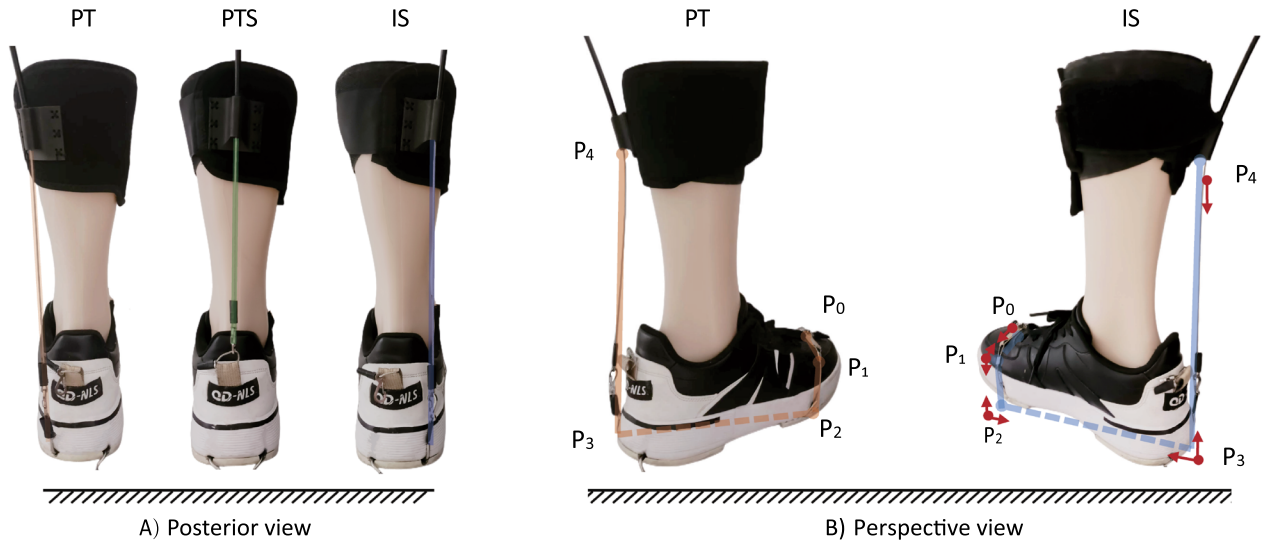

Fig. 3 The multi-dimensional views of three ankle exosuits. **A** The posterior view of the PT, PTS, and IS ankle exosuits, with the drive cable on the medial, middle, and lateral aspects of the right leg, respectively. **B** The perspective view of the IS and PT exosuits, including the points and direction of equivalent forces application. The cable arrangement is depicted as a solid and dashed line, representing the visible and invisible parts, respectively. The red arrows signify the direction of the force for the given points

the cable is securely fastened by looping it around the dorsal surface of the foot.

The PT scheme is a symmetrical arrangement with the IS scheme. After passing through the calf wrap, it follows a parallel path to the calf and extends toward the medial side of the heel, maintaining a distance of approximately 3 cm from the midpoint of the heel. At the sole, the PT's cable intersects with the IS's cable before continuing toward the fifth metatarsophalangeal joint. Finally, the PT cable is securely fastened to the dorsal surface of the foot.

The PTS scheme is arranged to mimic the triceps surae muscle. It runs parallel to the calf and is fixed at the center of the heel.

Control

The Bowden cable is an elastic component with complex surface friction characteristics, which can lead to the occurrence of nonlinear phenomena such as hysteresis and backlash during control. To address this issue, a p-type iterative learning algorithm is used in our study to track the assist force. In the experiment, the error of assist force from the current cycle is measured to correct the moment of the motor output shaft in the subsequent gait cycle. The targeted assist force is reached by persistently iterating.

Based on the moment of ankle active plantarflexion, we designed the assist force to an unimodal curve (Fig. 2A). The cycle duration is set to 5 s. During the first second of the cycle, the cable is maintained in a state of tension, with a tension force of 5N. Then, the tension force increases to 50N over a duration of 0.8 s. Once the peak value is attained, the cable payout process can be completed within 0.25 s. Finally, the cable remains under tension until the end of the cycle.

The dynamics of the ankle exosuits

1) Calculate the assistance moment unconsidering the ankle joint axes

The effects of the exosuits on the ankle joint can be equivalent to the application of five forces. These forces are applied at fixed and inflection points of the cable (Fig. 3B). The first point of force application, P_0, represents the fixed point of the cable on the dorsal surface of the foot. The second and third points of force application, P_1 and P_2 respectively, represent the inflection points where the cable changes direction from the upper to the side surface and then from the side to the sole. The fourth point of force application, P_3, indicates the fixed point on the heel. The entry point of the cable on the calf wrap is marked as P_4. The PTS can be considered a special scheme where P_0, P_1, P_2, and P_3 coincide at the heel.

In the superior view of the foot-ankle complex, the center of ankle joint rotation serves as the origin of the coordinate system $\{A\}$, as depicted in Fig. 1. In this coordinate system, the coordinates of the five points are as follows:

$$P_{i0} = \left(P_{i0}(x), P_{i0}(y), P_{i0}(y)\right), i = 0, 1, 2, 3, 4 \quad (1)$$

As the ankle motion during exosuits assistance, the coordinates of the five points will change correspondingly. Assuming that the ankle joint rotates θ_x, θ_y, and θ_z relative to the three axes of X_A-axis,Y_A-axis, and Z_A-axis, respectively, the coordinates of the five points after the rotation will be:

$$\begin{aligned} P_i &= R_z(\theta_z)R_y(\theta_y)R_x(\theta_x)P_{i0}, i = 0,1,2,3 \\ P_4 &= P_{40} \end{aligned} \tag{2}$$

where, $R_i(\theta_i)$ represents the rotation matrix that rotates around the i-axis by an angle θ_i. Since the calf is fixed, there is no coordinate change in P_4.

Assuming that the tension F is equal at each point along the cable without considering friction, the forces F_i acting on the ankle are:

$$\begin{aligned} F_0 &= F\frac{\overrightarrow{P_0P_1}}{\left|\overrightarrow{P_0P_1}\right|} \\ F_1 &= F\frac{\overrightarrow{P_1P_0}}{\left|\overrightarrow{P_1P_0}\right|} + F\frac{\overrightarrow{P_1P_2}}{\left|\overrightarrow{P_1P_2}\right|} \\ F_2 &= F\frac{\overrightarrow{P_2P_1}}{\left|\overrightarrow{P_2P_1}\right|} + F\frac{\overrightarrow{P_2P_3}}{\left|\overrightarrow{P_2P_3}\right|} \\ F_3 &= F\frac{\overrightarrow{P_3P_2}}{\left|\overrightarrow{P_3P_2}\right|} + F\frac{\overrightarrow{P_3P_4}}{\left|\overrightarrow{P_3P_4}\right|} \end{aligned} \tag{3}$$

where F_i is the force at P_i.

The assistance moment, denoted as M_{ank1}, is calculated by the sum of the forces cross multiplied by their respective moment arms about the ankle joint. This is expressed as:

$$M_{\text{ank1}} = \overrightarrow{OP_0} \times F_0 + \overrightarrow{OP_1} \times F_1 + \overrightarrow{OP_2} \times F_2 + \overrightarrow{OP_3} \times F_3 \tag{4}$$

where O is the origin of the coordinate system $\{A\}$.

2) Calculate the assistance moment considering the ankle joint axes

Due to the non-orthogonality of the ankle joint axes, the assistance moment of the ankle response may differ from the assistance moment input by the exosuit. To understand this difference, our study calculated the assistance moment of the ankle joint response based on the characteristics of the ankle joint axis. Specifically, we independently calculated the assist moments for the talocrural and subtalar joints and then added them together to determine the overall assist moment to the ankle.

To calculate the assistance moment on the subtalar joint, a new coordinate system $\{B\}$ was constructed by rotating the original coordinate system $\{A\}$. In this new system, the X_B-axis aligns with the axis of the subtalar joint, and the assistive moment on the subtalar joint is the moment acting on the X_B-axis (Fig. 1).

First, we solved the coordinates of the force application points in the coordinate system $\{B\}$. The subtalar joint's rotation axis is known to form an angle of $\varphi_z = 16°$ with the sagittal plane and an angle of $\varphi_x = 42°$ with the horizontal plane. Using geometric relations, we obtained the rotation matrix and the force application point coordinates in the coordinate system $\{B\}$:

$$P_{\text{isubtalar}} = R_y(\varphi_y)R_z(\varphi_z)P_i, i = 0,1,2,3,4 \tag{5}$$

where,

$$\begin{aligned} R_z(\varphi_z) &= [\cos(\varphi_z), \sin(\varphi_z), 0; -\sin(\varphi_z), \cos(\varphi_z), 0; 0, 0, 1] \\ R_y(\varphi_y) &= \left[\cos(\varphi_y), 0, -\sin(\varphi_y); 0, 1, 0; \sin(\varphi_y), 0, \cos(\varphi_y)\right] \\ \cos(\varphi_y) &= \frac{\sqrt{\tan^2(\varphi_z)+1}}{\sqrt{\tan^2(\varphi_z)+\tan^2(\varphi_x)+1}} \\ \sin(\varphi_y) &= -\frac{\tan(\varphi_x)}{\sqrt{\tan^2(\varphi_z)+\tan^2(\varphi_x)+1}} \end{aligned}$$

Then, we substituted the coordinates of $P_{\text{isubtalar}}$ into Eq.(3, 4) to solve the subtalar joint moment M^B_{subtalar} under the coordinate system $\{B\}$.

Finally, we projected the subtalar joint moment onto the coordinate system $\{A\}$:

$$M^A_{\text{subtalar}} = R_z(\varphi_z)'R_y(\varphi_y)'M^B_{\text{subtalar}}[1,0,0]' \tag{6}$$

where, $R_z(\varphi_z)'$ and $R_y(\varphi_y)'$ are the inverses of $R_z(\varphi_z)$ and $R_y(\varphi_y)$.

Similarly, we calculated the moment on the talocrural joint by rotating the original coordinate system $\{A\}$ to the coordinate system $\{C\}$, where the Y_C-axis aligns with the talocrural joint axis. By determining the exosuit moment on the Y_C-axis in the coordinate system $\{C\}$, we calculated the talocrural joint moment.

To begin, we solved for the coordinates of the force application points in the coordinate system $\{C\}$. The rotation axis of the talocrural joint forms an angle of $\beta_x = 6°$ with the frontal plane, and forms an angle of $\beta_y = 10°$ with the horizontal plane. Using geometric relations, we obtained the rotation matrix and the point coordinates after rotation in the coordinate system $\{C\}$:

$$P_{\text{italocrural}} = R_z(\beta_z)R_x(\beta_x)P_i, i = 0,1,2,3,4 \tag{7}$$

where,

$$R_x(\beta_x) = [1, 0, 0;\ \cos(\beta_x), \sin(\beta_x), 0;\ 0, -\sin(\beta_x), \cos(\beta_x)]$$
$$R_z(\beta_z) = [\cos(\beta_z), \sin(\beta_z), 0;\ -\sin(\beta_z), \cos(\beta_z), 0;\ 0, 0, 1]$$
$$\cos(\beta_z) = \frac{\sqrt{\tan^2(\beta_y) + 1}}{\sqrt{\tan^2(\beta_x) + \tan^2(\beta_y) + 1}}$$
$$\sin(\beta_z) = -\frac{\tan(\beta_x)}{\sqrt{\tan^2(\beta_x) + \tan^2(\beta_y) + 1}}$$

Next, we substituted $P_{\text{italocrural}}$ into the Eq.(3, 4) to solve the moment $M^C_{\text{talocrural}}$.

Finally, we projected the talocrural joint moment onto the coordinate system $\{A\}$:

$$M^A_{\text{talocrural}} = R_x(\beta_x)' R_z(\beta_z)' M^C_{\text{talocrural}} [0, 1, 0]' \quad (8)$$

where, $R_z(\beta_z)'$ and $R_x(\beta_x)'$ are the inverses of $R_z(\beta_z)$ and $R_x(\beta_x)$.

In summary, the comprehensive moment M_{ank2} of the exosuit to the ankle joint is obtained:

$$\begin{aligned} M_{\text{ank2}} &= M^A_{\text{subtalar}} + M^A_{\text{talocrural}} \\ &= f\left(P_{30}, F, \theta_x, \theta_y, \theta_z\right). \end{aligned} \quad (9)$$

The detailed calculation process and results are documented in the supplementary materials. MATLAB (MathWorks Inc., USA) was used for solving the formulas.

Simulation protocol

In our study, the simulation calculated the assistance moment curve under two conditions: one considering the ankle axes using Eq. (9) and the other without using Eq. (4). The applied assistive force was held constant at 1, and the coordinates of point P_{30} were (−0.09, ± 0.03, −0.11). The ankle angle curves used as model inputs are presented below:

$$\theta_q = \theta_{\text{qmax}} \sin(t)(q = x, y, z), \quad 0 < t < \pi \quad (10)$$

where θ_{qmax} denoted the maximum ankle angle in the q-axis during the exosuit assist experiments. All results are dimensionless.

Participants

Seven adult males completed the experiment (20.1 ± 3.1 years, 178 ± 35 cm, 72.0 ± 7.1kg). All participants provided informed consent and were informed of the possible consequences of the study. The Science and Technology Committee of Huazhong University of Science and Technology approved the experimental protocol for using human subjects.

Experimental protocol

Participants were instructed to wear the exosuit on their right leg and sit on a table to complete ankle plantarflexion. To reduce the impact from rotation from the hip and knee joints, the strap was utilized to secure the participants' right leg to the platform. The experiment consisted of four tests: an active ankle plantarflexion motion and three passive ankle plantarflexion motions assisted by PT, PTS, and IS, respectively. During the active test, participants were directed to actively perform ankle plantarflexion, following the operator's commands. The exosuit was worn but not actuated, and did not impede ankle joint motion. During the three passive ankle plantarflexion tests, participants were instructed to consistently maintain a relaxed state while completing plantarflexion with the assistance of the exosuit. Each cycle lasted for five seconds, and participants repeated ankle plantarflexion movements at least 20 times during each test.

While seated, the initial ankle position was defined with the soles of the feet parallel to the ground, maintaining a 90° angle between the calf and sole. Throughout the experiment, participants were instructed to monitor the motion of their ankle joints by a mirror and make an effort to return the ankle joint to its initial position before each plantarflexion.

Measurements and data processing

Kinematic data of the ankle in three dimensions were collected using a 7-camera reflective marker motion capture system (Vicon, Oxford Metrics, Oxford, UK; 100 Hz). Seven infrared reflective markers were placed on specific anatomical landmarks on the right leg, including the lateral knee joint (P_{knee}), medial/lateral malleolus ($P_{\text{ankle\_med}}/P_{\text{ankle\_lat}}$), heel ($P_{\text{heel}}$), and 1st, 2nd, and 5th metatarsophalangeal joints ($P_{\text{toe1}}, P_{\text{toe2}}, P_{\text{toe5}}$). The three-dimensional coordinates of each marker were filtered with a 6-Hz low pass Butterworth filter.

The three-dimensional angle of the ankle joint was calculated according to geometric relationships:

$$
\begin{aligned}
\theta_{\mathrm{IN}} &= \arccos\left(\frac{\overrightarrow{leg_{\parallel}}\cdot\overrightarrow{foot_{\perp}}}{\left|\overrightarrow{leg_{\parallel}}\right|\left|\overrightarrow{foot_{\perp}}\right|}\right)-\frac{\pi}{2}\\
\theta_{\mathrm{AD}} &= \arccos\left(\frac{\overrightarrow{foot_{\parallel}}\cdot\overrightarrow{leg_{\perp}}}{\left|\overrightarrow{foot_{\parallel}}\right|\left|\overrightarrow{leg_{\perp}}\right|}\right)-\frac{\pi}{2}\\
\theta_{\mathrm{PF}} &= \arccos\left(\frac{\overrightarrow{foot_{\parallel}}\times\overrightarrow{leg_{\perp}}\cdot\overrightarrow{leg_{\parallel}}}{\left|\overrightarrow{leg_{\parallel}}\right|\left|\overrightarrow{foot_{\parallel}}\times\overrightarrow{leg_{\perp}}\right|}\right)
\end{aligned}
\tag{11}
$$

$$
\begin{aligned}
\overrightarrow{leg_{\parallel}} &= P_{\mathrm{knee}} - P_{\mathrm{ankle\_lat}}\\
\overrightarrow{leg_{\perp}} &= P_{\mathrm{ankle\_med}} - P_{\mathrm{ankle\_lat}}\\
\overrightarrow{Foot_{\parallel}} &= P_{\mathrm{toe2}} - P_{\mathrm{heel}}\\
\overrightarrow{Foot_{\perp}} &= P_{\mathrm{toe1}} - P_{\mathrm{toe5}}
\end{aligned}
$$

where, θ_{IN}, θ_{AD}, and θ_{PF} are the inversion, adduction, and plantarflexion angles of the ankle, respectively. The data from the last one minute was collected. The curves of ankle angle from each condition were averaged across participants.

Statistical analysis

We utilized Dynamic Time Warping (DTW) to calculate the trajectory distance between the three exosuit-assisted motions and active motion. Statistical analysis involved Bland-Altman plots to assess differences between the three exosuit-assisted motions and active motion. Additionally, statistical analyses were conducted on the linear correlation coefficients of angles in pairwise orthogonal directions and peak values of ankle angles in three directions. The normal distribution assumption was assessed using the Jarque-Bera two-sided goodness test. A one-way repeated-measures analysis of variance (ANOVA) was employed to evaluate differences between active and passive ankle plantarflexion, excluding outliers with a Thompson Tau test. The significance level for all analyses was set at $P < 0.05$. We also conducted a power analysis to determine the probability of a Type II error. Our acceptance criteria for power levels ranged from 0.80 or higher. Effect sizes (ES) were calculated using Cohen's d, which is defined as the difference of group means divided by the pooled standard deviation. This allowed us to quantify the difference between active and passive ankle plantarflexion, with an effect size of 0.2 considered small, 0.5 medium, and 0.8 large. All statistical analyses were performed using MATLAB (MathWorks Inc., USA).

Results

The ankle moments generated by the PT, PTS, and IS exosuits significantly differ when considering the non-orthogonal characteristics of ankle joint axes compared to not considering them, assuming the ankle joint maintains its initial position. Without considering the ankle joint axes, the moments for plantarflexion all are 0.090, inversion are 0.030 (PT), 0.000 (PTS), and −0.030 (IS), with all zero adduction moments. When considering the ankle joint axes, the ankle moments change as follows: plantarflexion moments of 0.0996 (PT), 0.0920 (PTS), and 0.0840 (IS), inversion moments of 0.039 (PT), 0.023 (PTS), and 0.007 (IS), and adduction moments of 0.036 (PT), 0.022 (PTS), and 0.007 (IS) (Fig. 4A–C).

Considering the changes in ankle joint angle during assistance, this study calculated the curve of assistance moments with ankle movement (Fig. 4D–F). The simulation results reveal that as the ankle angle increased, the plantarflexion, inversion, and adduction moments provided by the exosuits increased in all three directions. Additionally, all simulation results for the moment curve displayed left-right symmetry, signifying that the magnitude of the exosuit assistive moment remained unaffected by the direction of ankle motion velocity.

We assessed the differences in ankle kinematics between the three exosuit-assisted motions and active motion through motion acquisition experiments (Fig. 5A–C). During the ankle active plantarflexion experiment, the peak angles for plantarflexion, inversion, and adduction were measured at 38.36±4.86 degrees, 6.26±3.59 degrees, and 8.62±4.94 degrees, respectively. In the ankle passive plantarflexion experiment, three different exosuits, PT, PTS, and IS, were utilized. The plantarflexion peak angles for the ankle assisted by these three exosuits were found to be 39.59±4.15 degrees, 38.41 ± 3.66 degrees, and 42.5 ± 4.46 degrees, respectively. The inversion peak angles were 28.17 ± 3.26 degrees, 13.83±1.46 degrees, and 10.79±3.89 degrees, while the adduction peak angles were 17.66±4.58 degrees, 11.66 ± 4.33 degrees, and 9.87±5.34 degrees, respectively (Fig. 5D–F; Table 2).

Using Bland-Altman plots, we observed that the three assistive motions show agreement across most motion ranges with active ankle motion. However, there is a clustering of outlier points before and after reaching the peak angle (Fig. 5D–F).

In the plots of the phase trajectory diagram, it was observed that both active ankle motion and exosuit-assisted motion demonstrate an increase in ankle inversion and adduction angles as the ankle plantarflexion angle increases and shows a clear linear correlation (Fig. 5G–I). During the active ankle plantarflexion

Table 2 The mean (standard deviation) and statistic analysis of the ankle peak angles and the linear correlation coefficients in four experimental schemes

Valve	Active	PTS				PT				IS			
	Mean(SD)	Mean(SD)	P-value	ES	Power	Mean(SD)	P-value	ES	Power	Mean(SD)	P-value	ES	Power
PF peak	38.36(4.86)	39.59(4.15)	0.62	− 0.27	0.09	38.41(3.66)	0.99	− 0.01	0.05	42.52(4.46)*	0.12	− 0.89	0.48
IN peak	6.26(3.59)	28.17(3.24)*	< 0.05	− 6.41	1.00	13.83(1.46)*	< 0.05	− 2.76	1.00	10.79(3.89)*	<0.05	− 1.21	0.79
AD peak	8.62(4.94)	17.66(4.58)*	< 0.05	− 1.90	0.98	11.66(4.33)	0.24	− 0.65	0.28	9.87(5.34)	0.66	− 0.24	0.09
IN/PF	0.22(0.13)	0.78(0.16)*	< 0.05	− 3.84	1.00	0.41(0.08)*	< 0.05	− 1.70	1.00	0.28(0.06)	0.42	− 0.54	0.99
AD/PF	0.22(0.08)	0.46(0.09)*	< 0.05	− 2.72	0.89	0.28(0.06)	0.27	− 0.75	0.30	0.22(0.04)	0.97	0.03	0.88
AD/IN	0.97(0.35)	1.69(0.23)*	< 0.05	− 2.45	0.16	1.47(0.16)*	< 0.05	− 1.84	0.05	1.28(0.31)*	0.18	− 0.93	0.50

* indicates that the value in the current scheme exhibits a significant difference compared to ankle active plantarflexion (P-value < 0.05 or |ES| > 0.8)

experiment, the linear correlation coefficients between the inversion angle and plantarflexion angle, between adduction angle and plantarflexion angle, and between adduction angle and inversion angle were 0.22 ± 0.13, 0.22 ± 0.08, and 0.97 ± 0.35, respectively. In the passive ankle plantarflexion experiment, the linear correlation coefficients between the inversion angle and plantarflexion angle for the three exosuits PT, PTS, and IS were 0.78 ± 0.16, 0.41 ± 0.08, and 0.28 ± 0.06, respectively. The linear correlation coefficients between the adduction angle and plantarflexion angle were 0.46 ± 0.09, 0.28 ± 0.06, and 0.22 ± 0.04, respectively. The linear correlation coefficients between the adduction angle and inversion angle were 1.69 ± 0.23, 1.47 ± 0.16, and 1.28 ± 0.31, respectively (Table 2).

When comparing the three schemes, the linear correlation coefficients of the IS scheme were found to be the closest to those of active ankle motion. No significant differences were observed between IS-assisted and active ankle motion regarding the coefficients between the inversion angle and plantarflexion angle, as well as between the adduction angle and plantarflexion angle. Within the PTS scheme, the linear correlation coefficients between the inversion angle and plantarflexion angle, as well as between the adduction angle and inversion angle, showed a statistically significant increase compared to active ankle motion ($P < 0.05$, or effect size: $|d| > 0.80$; Table 2). Similarly, the three linear correlation coefficients for the PT demonstrated a statistical increase, with larger effect sizes observed in all three directions compared to PTS.

The similarity of ankle angle curves was assessed using DTW distances. In the PT scheme, the mean DTW distances to the active ankle plantarflexion angle curve were 1.02°, 7.78°, and 1.65° in the plantarflexion, inversion, and adduction directions, respectively (see Table 3). The root mean square distance across the three directions totaled 4.63°. In the PTS scheme, the corresponding curve distances measured 0.93°, 2.62°, and 0.91° in the plantarflexion, inversion, and adduction directions, respectively, with a root mean square distance of 1.69°. Within the IS scheme, the curve distances were 1.55°, 1.79°, and 0.25° in the plantarflexion, inversion, and adduction directions, respectively, with a root mean square distance of 1.37°. Overall, compared to the other two schemes, the IS scheme exhibited the smallest curve distances to active ankle plantarflexion.

Discussion

In this study, three exosuits, the PT, IS, and PTS, were developed based on the ankle joint axes and muscle distribution. We investigated the impact of the position and direction of the force line on the ankle's three-dimensional motion. This was done to identify an ankle exosuit design that can provide a more natural form of assistance.

A dynamic model was developed to calculate the exosuit assistance moment. Simulation results revealed that all three schemes generated a plantarflexion moment by positioning the force line posterior to the talocrural joint axis. Among these schemes, the PT scheme, with the longest moment arm relative to the two joint axes, yielded the highest moment for these axes. Moreover, both the PT and PTS schemes induced ankle inversion and adduction moments by influencing subtalar joint motion. The PTS scheme exhibited a lower non-plantarflexion moment due to its shorter moment arm to the subtalar joint compared to the PT scheme. Conversely, the IS scheme, intersecting with or near the subtalar joint axis, had a minimal moment arm for subtalar joint motion. Consequently, the IS scheme displayed the smallest non-plantarflexion moment compared to the other two schemes.

During the exosuit assistance, the moment arm increases with the ankle plantarflexion angle, which in turn enlarges the moment and yields a larger angle of

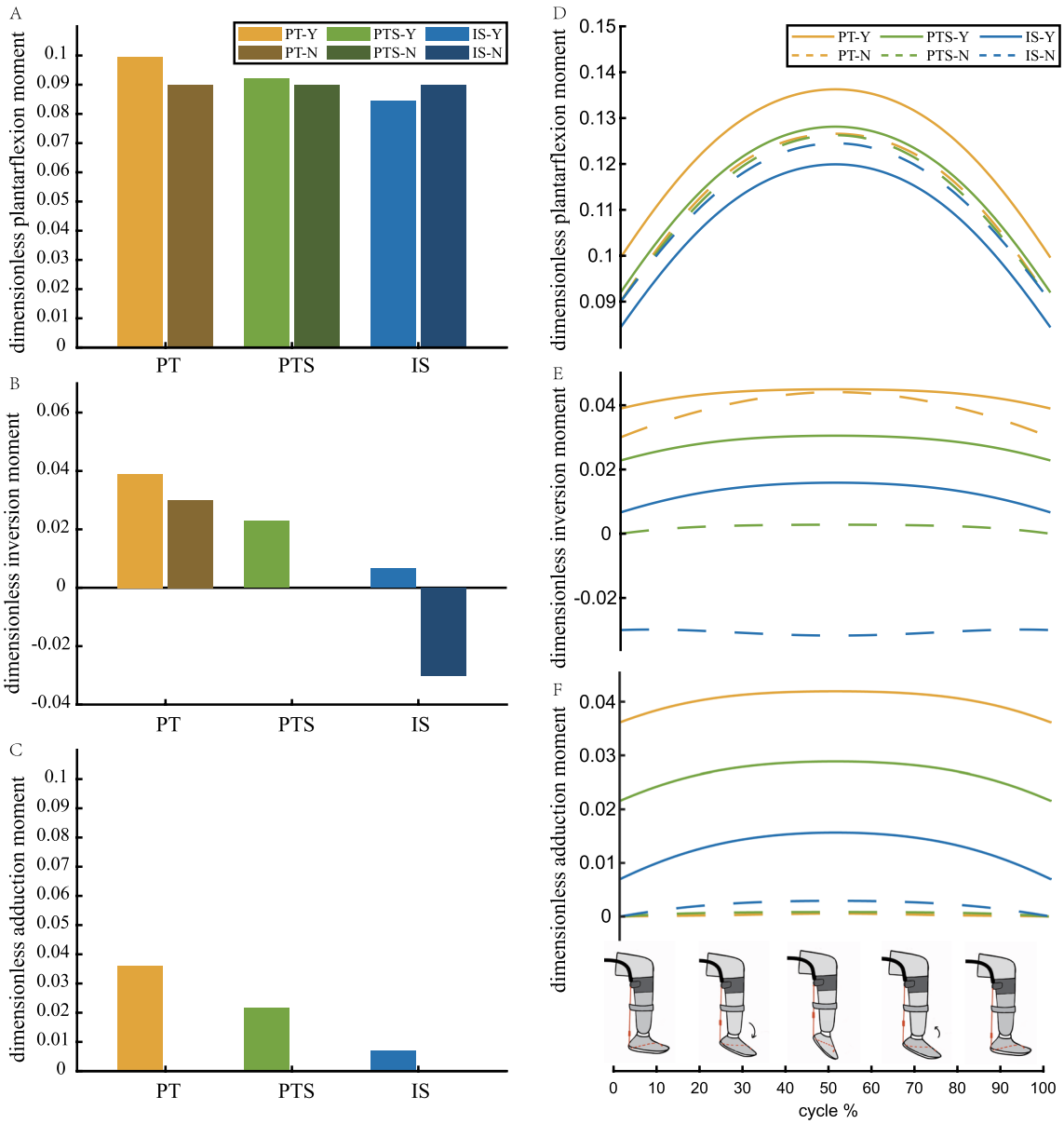

Fig. 4 The assistance moments of the three exosuits. A-C) The non-dimensional assistance moments of plantarflexion, inversion, and adduction with the ankle maintain a plantarflexion angle of 0°, respectively. D-F) The non-dimensional assistance moments curves of plantarflexion, inversion, and adduction with ankle motion, respectively. The notation "-Y" indicates that the ankle axes were considered in the analysis, while "-N" indicates that they were neglected

motion. That is more obvious in the PT scheme. When plantarflexion and inversion moments are generated by the ankle exosuit, corresponding plantarflexion, and inversion motion of the ankle are induced. Then, as the ankle inversion angle increases, the exosuit's inversion moment arm of the assistance force line also increases, leading to a further increase in the inversion moment. The lateral collateral ligaments limit ankle inversion while the triangular ligament limits ankle eversion. Given the lateral collateral ligaments are weaker than the triangular ligament and the inversion motion range is larger than eversion (23° inversion, -12° eversion) [42], ankle sprains often involve ankle inversion [43, 44]. Therefore, the ankle inversion moment provided by ankle exosuits should be carefully applied.

In previous experiments conducted by Ho Seon Choi and colleagues [36, 45], they observed that a 1-DOF powered ankle-foot orthosis, which shares structural

Table 3 The mean DTW distances (°) of angle curves between the three exosuit-assisted motions and active motion

Rotation	PT	PTS	IS
PF(+)/DF(−)	1.02	0.93	1.55
IN(+)/EN(−)	7.78	2.62	1.79
AD(+)/AB(−)	1.65	0.91	0.25
RMS[a]	4.63	1.69	1.37

[a] RMS stands for the square root of the mean distance calculated in three directions

similarity with the PTS scheme, resulted in a lateral shift of the in-shoe center of pressure during walking. Their results indicated that the 1-DOF-powered ankle-foot orthosis could generate unexpected inversion moments. These findings align with our simulation and experimental results, in which the PTS scheme generated an inversion moment at the ankle joint.

We investigated the differences in ankle kinematics resulting from three exosuit schemes through exosuit-assisted experiments, and the findings were consistent with the simulation results. All three schemes effectively assisted ankle plantarflexion. The PT scheme exhibited the largest increase in the peak angle of ankle inversion and adduction, followed by PTS and IS. This difference can be attributed to the fact that the PT scheme introduced the highest ankle non-plantarflexion moments, followed by the PTS and IS schemes. In contrast, the IS assistance produced the smallest peak angles for ankle inversion and adduction among the three schemes, along with the smallest DTW distance and the highest similarity to active plantarflexion.

We observed that the differences in ankle joint motion between three exosuit-assisted and active ankle motions mainly clustered before and after reaching the peak angle. This phenomenon can be attributed to the fact that, with assistance, the plantarflexion velocity of the ankle joint surpasses that of active motion. Consequently, the ankle joint reaches its limit position earlier with assistance compared to active motion, resulting in differences around the joint limit position. The coordination among the multidimensional movements of the ankle joint, rather than differences in velocity along individual movement directions, enables a clearer understanding of the impact of assistive force lines on natural ankle joint motion. Therefore, we proposed conducting further analysis of the differences in ankle joint motion across three directions between assisted and active motion using phase trajectories. From the phase plots, it was observed that as the force lines approached the subtalar joint axis, the linear correlation coefficients gradually converged towards the coefficients of active ankle joint motion.

Additionally, we need to clarify why we opted for a relatively large assistive force magnitude. The decision stemmed from the need for consistency and repeatability in our experiments. Participants were instructed to achieve the maximum plantarflexion angle possible during active ankle motion, ensuring consistent peak angles across multiple cycles. Simultaneously, to ensure that all participants achieved maximal ankle joint movement during exosuit-assisted motion, we set the peak assistive force at a relatively high level of 50N across multiple experimental trials. This applied force resulted in a notably higher plantarflexion velocity of the ankle joint compared to that observed during active motion.

In summary, this study indicates that the IS scheme has the least interference with non-plantarflexion movements and is closest to natural ankle joint motion compared to the other two schemes. Considering the ankle's crucial role in maintaining lateral balance through actively generating inversion and eversion moments [16, 19], the IS exosuit provides the flexibility needed to support ankle inversion and eversion motions, making it a promising candidate for future applications.

Due to individual differences in the direction of ankle joint axes [46], the lines of assistance force produced by our exosuits may not be precisely perpendicular to the talocrural joint or intersect with the subtalar joint. For example, we assumed that the axis of the talocrural joint formed a 10° angle with respect to the sagittal plane based on prior research [47, 48]. However, some studies have shown that this angle can vary between 6° and 4° among different subjects [46, 49]. Nevertheless, these variations do not impact the validity of our research plan or primary conclusions. The three force lines always satisfy the following conditions: the PT has the largest force arm relative to the two axes, followed by the PTS, and then the IS.

We obtained the current findings from a sample consisting of male participants. Considering the differences in male and female biology and physiology [50, 51], we will investigate potential gender-related variations among three assistance schemes in future work.

Conclusions

The talocrural and subtalar joints are the major rotation joints for the ankle joint complex. The assistance force line of the exosuit relative to these two joint axes is essential for ankle motion. In this study, we proposed three bionic force line schemes: perpendicular to the talocrural joint (PT), intersecting with the subtalar joint axis (IS), and parallel to the triceps calf (PTS). We conducted simulations and experiments to assess the impact of different force line configurations on

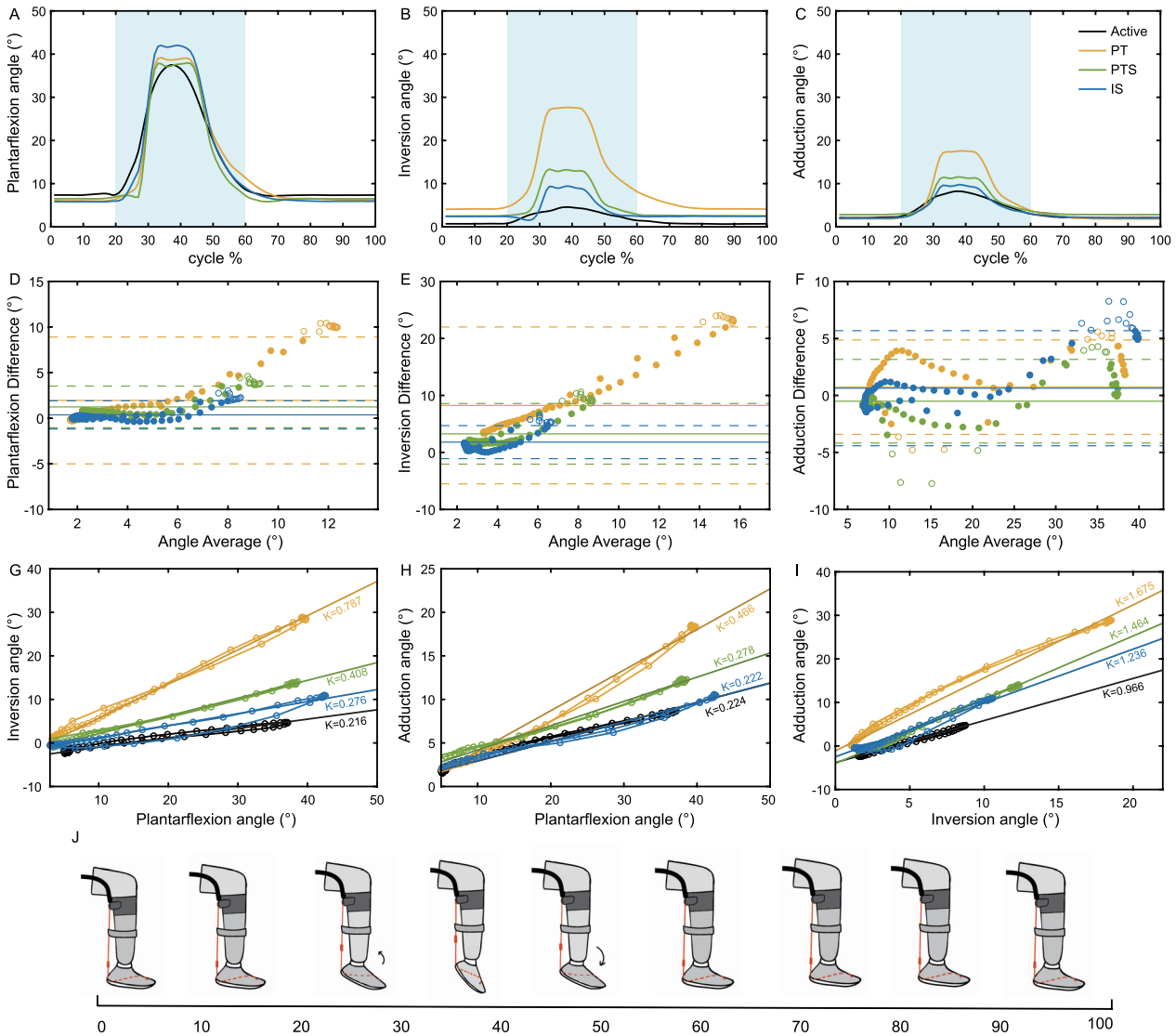

Fig. 5 Ankle motion analysis. **A**–**C** show the average angle across a motion cycle of the ankle in the directions of plantarflexion, inversion, and adduction, respectively. **D**–**F** depict the motion differences between three exosuit-assisted and active ankle motions in the directions of plantarflexion, inversion, and adduction, utilizing Bland-Altman plots. In these plots, circles represent the angle differences of the three assistive motions relative to active ankle motion. Solid markers indicate differences within the limits, while hollow markers indicate differences beyond the limits. The horizontal dashed lines represent the limits of agreement, corresponding to the mean angle difference ± 1.96 standard deviations of angle differences, while the solid horizontal lines represent the mean angle difference. **G**–**I** illustrate the phase trajectory of ankle motion between the inversion angle and plantarflexion angle, between the adduction angle and plantarflexion angle, and between the adduction angle and inversion angle, respectively. The K value denotes the trajectory s slope, representing the linear correlation coefficient between the two angles. **J** presents a schematic representation of ankle motion in a motion cycle. Each color corresponds to a specific experiment condition: black for active plantarflexion without exosuit assistance (Active), blue for IS assistance, green for PTS assistance, and yellow for PT assistance. The light blue rectangle represents the primary region of ankle motion

multidimensional ankle motion. Our findings reveal that all three schemes effectively assisted ankle plantarflexion. As the assistive force lines approached the subtalar joint axis, exosuit-assisted motion in the non-plantarflexion direction decreased, the distance of ankle angle curves relative to active ankle motion decreased, and the linear correlation coefficients also gradually converged towards active ankle plantarflexion motion. In summary, the IS scheme exhibits the highest kinematic similarity to active ankle plantarflexion compared to the other two schemes, making it the optimal choice for ankle assistance and rehabilitation.

Abbreviations

PT	Perpendicular to the talocrural joint axis
IS	Intersecting with the subtalar joint axis
PTS	Parallel to the triceps surae
ES	Effect sizes
DTW	Dynamic Time Warping
IN	Inversion
PF	Plantarflexion
AD	Adduction

Supplementary Information

The online version contains supplementary material available at https://doi.org/10.1186/s12984-024-01386-x.

Additional file 1. Ankle plantarflexion with PT exosuit assistance An illustrative video for understanding pre-experiment.

Additional file 2. Exosuit assistance moments - Detailed derivation process and results.

Acknowledgements
The authors thank Qin Zhang for helping revise the manuscript. Peng Xun and KaiJie Zou for assisting in developing the exosuit system.

Author contributions
Ronglei Sun and Xinyue Zhang proposed the three ankle exosuit schemes and designed the experiments. Xinyue Zhang and Ying Li designed the control algorithm, performed the biomechanics experiments, and processed the data. Ronglei Sun, Xinyue Zhang, and Ying Li interpreted the results of the study. Xinyue Zhang drafted the manuscript, and Xinyue Zhang, Ying Li, and Ronglei Sun edited and revised the manuscript. All authors gave their final approval for publication.

Funding
This work was supported by the National Natural Science Foundation of China (Grant No. U21A20121, Grant No. 52027806)

Availability of data and materials
The data collected and analyzed in the current study are available in the manuscript and supplementary data. More details are available from the corresponding author upon request.

Declarations

Ethics approval and consent to participate
All participants provided informed consent before their participation and the possible consequences of the studies were explained. The experimental protocol was approved by the Huazhong University of Science and Technology Committee on the use of humans as experimental subjects.

Consent for publication
Not applicable.

Competing interests
The authors declare that they have no competing of interests.

Received: 29 October 2023 Accepted: 15 May 2024
Published online: 28 May 2024

References

1. Brockett CL, Chapman GJ. Biomechanics of the ankle. Orthop Trauma. 2016;30(3):232–8. https://doi.org/10.1016/j.mporth.2016.04.015.
2. Kulmala JP, Korhonen MT, Ruggiero L, Kuitunen S, Suominen H, Heinonen A, Mikkola A, Avela J. Walking and running require greater effort from the ankle than the knee extensor muscles. Med Sci Sports Exerc. 2016;48(11):2181–9. https://doi.org/10.1249/MSS.0000000000001020.
3. McGowan CP, Neptune RR, Kram R. Independent effects of weight and mass on plantar flexor activity during walking: implications for their contributions to body support and forward propulsion. J Appl Physiol (1985). 2008;105(2):486–94. https://doi.org/10.1152/japplphysiol.90448.2008.
4. Zhang J, Fiers P, Witte KA, Jackson RW, Poggensee KL, Atkeson CG, Collins SH. Human-in-the-loop optimization of exoskeleton assistance during walking. Science. 2017;356(6344):1280–4. https://doi.org/10.1126/science.aal5054.
5. Gasparri GM, Luque J, Lerner ZF. Proportional joint-moment control for instantaneously adaptive ankle exoskeleton assistance. IEEE Trans Neural Syst Rehabil Eng. 2019;27(4):751–9. https://doi.org/10.1109/TNSRE.2019.2905979.
6. Gordleeva SY, Lobov SA, Grigorev NA, Savosenkov AO, Shamshin MO, Lukoyanov MV, Khoruzhko MA, Kazantsev VB. Real-time EEG-EMG human-machine interface-based control system for a lower-limb exoskeleton. IEEE Access. 2020;8:84070–81. https://doi.org/10.1109/access.2020.2991812.
7. Sanchez-Villamanan MDC, Gonzalez-Vargas J, Torricelli D, Moreno JC, Pons JL. Compliant lower limb exoskeletons: a comprehensive review on mechanical design principles. J Neuroeng Rehabil. 2019;16(1):55. https://doi.org/10.1186/s12984-019-0517-9.
8. Nuckols RW, Lee S, Swaminathan K, Orzel D, Howe RD, Walsh CJ. Individualization of exosuit assistance based on measured muscle dynamics during versatile walking. Sci Robot. 2021;6(60):1362. https://doi.org/10.1126/scirobotics.abj1362.
9. Schmitz DG, Nuckols RW, Lee S, Akbas T, Swaminathan K, Walsh CJ, Thelen DG. Modulation of achilles tendon force with load carriage and exosuit assistance. Sci Robot. 2022;7(71):1514. https://doi.org/10.1126/scirobotics.abq1514.
10. Gonzalez S, Stegall P, Cain SM, Siu HC, Stirling L. Assessment of a powered ankle exoskeleton on human stability and balance. Appl Ergon. 2022;103:103768. https://doi.org/10.1016/j.apergo.2022.103768.
11. Fang Y, Lerner ZF. Feasibility of augmenting ankle exoskeleton walking performance with step length biofeedback in individuals with cerebral palsy. IEEE Trans Neural Syst Rehabil Eng. 2021;29:442–9. https://doi.org/10.1109/TNSRE.2021.3055796.
12. Grimmer M, Quinlivan BT, Lee S, Malcolm P, Rossi DM, Siviy C, Walsh CJ. Comparison of the human-exosuit interaction using ankle moment and ankle positive power inspired walking assistance. J Biomech. 2019;83:76–84. https://doi.org/10.1016/j.jbiomech.2018.11.023.
13. Sawicki GS, Beck ON, Kang I, Young AJ. The exoskeleton expansion: improving walking and running economy. J Neuroeng Rehabil. 2020;17(1):25. https://doi.org/10.1186/s12984-020-00663-9.
14. Miller DE, Tan GR, Farina EM, Sheets-Singer AL, Collins SH. Characterizing the relationship between peak assistance torque and metabolic cost reduction during running with ankle exoskeletons. J Neuroeng Rehabil. 2022;19(1):46. https://doi.org/10.1186/s12984-022-01023-5.
15. Kao PC, Lewis CL, Ferris DP. Invariant ankle moment patterns when walking with and without a robotic ankle exoskeleton. J Biomech. 2010;43(2):203–9. https://doi.org/10.1016/j.jbiomech.2009.09.030.
16. Arndt A, Westblad P, Winson I, Hashimoto T, Lundberg A. Ankle and subtalar kinematics measured with intracortical pins during the stance phase of walking. Foot Ankle Int. 2004;25(5):357–64. https://doi.org/10.1177/107110070402500514.
17. Leardini A, O'Connor JJ, Giannini S. Biomechanics of the natural, arthritic, and replaced human ankle joint. J Foot Ankle Res. 2014;7(1):8. https://doi.org/10.1186/1757-1146-7-8.
18. Medina McKeon JM, Hoch MC. The ankle-joint complex: a kinesiologic approach to lateral ankle sprains. J Athl Train. 2019;54(6):589–602. https://doi.org/10.4085/1062-6050-472-17.
19. Jenkyn TR, Shultz R, Giffin JR, Birmingham TB. A comparison of subtalar joint motion during anticipated medial cutting turns and level walking using a multi-segment foot model. Gait Posture. 2010;31(2):153–8. https://doi.org/10.1016/j.gaitpost.2009.09.016.
20. Goto A, Moritomo H, Itohara T, Watanabe T, Sugamoto K. Three-dimensional in vivo kinematics of the subtalar joint during dorsi-plantarflexion and inversion-eversion. Foot Ankle Int. 2009;30(5):432–8. https://doi.org/10.3113/FAI-2009-0432.

21. Galle S, Malcolm P, Collins SH, De Clercq D. Reducing the metabolic cost of walking with an ankle exoskeleton: interaction between actuation timing and power. J Neuroeng Rehabil. 2017;14(1):35. https://doi.org/10.1186/s12984-017-0235-0.
22. Jastifer JR, Gustafson PA. The subtalar joint: biomechanics and functional representations in the literature. Foot (Edinb). 2014;24(4):203–9. https://doi.org/10.1016/j.foot.2014.06.003.
23. Gates DH, Aldridge JM, Wilken JM. Kinematic comparison of walking on uneven ground using powered and unpowered prostheses. Clin Biomech (Bristol, Avon). 2013;28(4):467–72. https://doi.org/10.1016/j.clinbiomech.2013.03.005.
24. Kim M, Collins SH. Step-to-step ankle inversion/eversion torque modulation can reduce effort associated with balance. Front Neurorobot. 2017;11:62. https://doi.org/10.3389/fnbot.2017.00062.
25. Ij T, Noten S, Lamoth CJ, Beek PJ, van der Woude LH, Houdijk H. Can external lateral stabilization reduce the energy cost of walking in persons with a lower limb amputation? Gait Posture. 2014;40(4):616–21. https://doi.org/10.1016/j.gaitpost.2014.07.013.
26. Steinberg N, Tenenbaum G, Witchalls J, Waddington G. The impact of unexpected platform perturbation on ankle proprioception ability in static and dynamic starting positions. Gait Posture. 2022;98:167–72. https://doi.org/10.1016/j.gaitpost.2022.09.003.
27. Cilli M, Serbest K, Kayaoglu E. The effect of body weight on joint torques in teenagers: investigation of sit-to-stand movement. Clin Biomech (Bristol, Avon). 2021;83: 105288. https://doi.org/10.1016/j.clinbiomech.2021.105288.
28. Baumhauer JF, Alosa DM, Renstrom AF, Trevino S, Beynnon B. A prospective study of ankle injury risk factors. Am J Sports Med. 1995;23(5):564–70. https://doi.org/10.1177/036354659502300508.
29. Willems TM, Witvrouw E, Delbaere K, Philippaerts R, De Bourdeaudhuij I, De Clercq D. Intrinsic risk factors for inversion ankle sprains in females-a prospective study. Scand J Med Sci Sports. 2005;15(5):336–45. https://doi.org/10.1111/j.1600-0838.2004.00428.x.
30. Kerr R, Arnold GP, Drew TS, Cochrane LA, Abboud RJ. Shoes influence lower limb muscle activity and may predispose the wearer to lateral ankle ligament injury. J Orthop Res. 2009;27(3):318–24. https://doi.org/10.1002/jor.20744.
31. Chiu VL, Voloshina AS, Collins SH. An ankle-foot prosthesis emulator capable of modulating center of pressure. IEEE Trans Biomed Eng. 2020;67(1):166–76. https://doi.org/10.1109/TBME.2019.2910071.
32. Kendrick D, Kumar A, Carpenter H, Zijlstra GA, Skelton DA, Cook JR, Stevens Z, Belcher CM, Haworth D, Gawler SJ, Gage H, Masud T, Bowling A, Pearl M, Morris RW, Iliffe S, Delbaere K. Exercise for reducing fear of falling in older people living in the community. Cochrane Database Syst Rev. 2014;2014(11): 009848. https://doi.org/10.1002/14651858.CD009848.pub2.
33. Schlick C, Schniepp R, Loidl V, Wuehr M, Hesselbarth K, Jahn K. Falls and fear of falling in vertigo and balance disorders: a controlled cross-sectional study. J Vestib Res. 2016;25(5–6):241–51. https://doi.org/10.3233/VES-150564.
34. Jamison M, Neuberger GB, Miller PA. Correlates of falls and fear of falling among adults with rheumatoid arthritis. Arthritis Rheum. 2003;49(5):673–80. https://doi.org/10.1002/art.11383.
35. Swaminathan K, Park S, Raza F, Porciuncula F, Lee S, Nuckols RW, Awad LN, Walsh CJ. Ankle resistance with a unilateral soft exosuit increases plantarflexor effort during pushoff in unimpaired individuals. J Neuroeng Rehabil. 2021;18(1):182. https://doi.org/10.1186/s12984-021-00966-5.
36. Choi HS, Baek YS, In H. Ankle strategy assistance to improve gait stability using controllers based on in-shoe center of pressure in 2 degree-of-freedom powered ankle-foot orthoses: a clinical study. J NeuroEng Rehabil. 2022;19(1):114. https://doi.org/10.1186/s12984-022-01092-6.
37. Jategaonkar C, Singh Y, Vashista V. Effect of external damping on ankle motion during the swing phase of walking. IEEE Robot Autom Lett. 2022;7(3):7612–9. https://doi.org/10.1109/lra.2022.3184781.
38. Awad LN, Bae J, O'Donnell K, De Rossi SMM, Hendron K, Sloot LH, Kudzia P, Allen S, Holt KG, Ellis TD, Walsh CJ. A soft robotic exosuit improves walking in patients after stroke. Sci Transl Med. 2017;9(400): eaai9084. https://doi.org/10.1126/scitranslmed.aai9084.
39. Xia HS, Kwon JH, Pathak P, Ahn J, Shull PB, Park YL. Design of a multifunctional soft ankle exoskeleton for foot-drop prevention, propulsion assistance, and inversion/eversion stabilization. In: Xia RS, editor. 2020 8th IEEE Ras/Embs international conference for biomedical robotics and biomechatronics (Biorob). New york: IEEE; 2020. p. 118–23.
40. Wang TM, Pei X, Hou TG, Fan YB, Yang X, Herr HM, Yang XB. An untethered cable-driven ankle exoskeleton with plantarflexion–dorsiflexion bidirectional movement assistance. Front Inform Technol Electr Eng. 2020;21(5):723–39. https://doi.org/10.1631/Fitee.1900455.
41. Lerner ZF, Gasparri GM, Bair MO, Lawson JL, Luque J, Harvey TA, Lerner AT. An untethered ankle exoskeleton improves walking economy in a pilot study of individuals with cerebral palsy. IEEE Trans Neural Syst Rehabil Eng. 2018;26(10):1985–93. https://doi.org/10.1109/TNSRE.2018.2870756.
42. Golano P, Vega J, de Leeuw PA, Malagelada F, Manzanares MC, Gotzens V, van Dijk CN. Anatomy of the ankle ligaments: a pictorial essay. Knee Surg Sports Traumatol Arthrosc. 2010;18(5):557–69. https://doi.org/10.1007/s00167-010-1100-x.
43. D'Hooghe P, Cruz F, Alkhelaifi K. Return to play after a lateral ligament ankle sprain. Curr Rev Musculoskelet Med. 2020;13(3):281–8. https://doi.org/10.1007/s12178-020-09631-1.
44. Kaminski TW, Needle AR, Delahunt E. Prevention of lateral ankle sprains. J Athl Train. 2019;54(6):650–61. https://doi.org/10.4085/1062-6050-487-17.
45. Choi HS, Baek YS. Effects of the degree of freedom and assistance characteristics of powered ankle-foot orthoses on gait stability. PLoS ONE. 2020;15(11):0242000. https://doi.org/10.1371/journal.pone.0242000.
46. Sheehan FT. The instantaneous helical axis of the subtalar and talocrural joints: a non-invasive in vivo dynamic study. J Foot Ankle Res. 2010;3:13. https://doi.org/10.1186/1757-1146-3-13.
47. Neumann DA. Kinesiology of the musculoskeletal system: foundations for rehabilitation. Amsterdam: Elsevier Health Sciences; 2016.
48. Zhao DH, Huang DC, Zhang GH, Fan YP, Yu J, Wang SB, Wang K, Ma X. Talar dome investigation and talocrural joint axis analysis based on three-dimensional (3d) models: Implications for prosthetic design. Biomed Res Int. 2019;2019:8634159. https://doi.org/10.1155/2019/8634159.
49. Claassen L, Luedtke P, Yao D, Ettinger S, Daniilidis K, Nowakowski AM, Mueller-Gerbl M, Stukenborg-Colsman C, Plaass C. The geometrical axis of the talocrural joint-suggestions for a new measurement of the talocrural joint axis. Foot Ankle Surg. 2019;25(3):371–7. https://doi.org/10.1016/j.fas.2018.02.003.
50. Kasim S. Effects of weight gaining to lower limb joint moments: a gender-specific sit-to-stand analysis. Biomed Eng. 2022;67(6):481–9. https://doi.org/10.1515/bmt-2022-0085.
51. Hudson S, Barwood M, Low C, Wills J, Fish M. A systematic review of the physiological and biomechanical differences between males and females in response to load carriage during walking activities. Appl Ergon. 2023;114: 104123. https://doi.org/10.1016/j.apergo.2023.104123.

Publisher's Note